Research Square

Preprints are preliminary reports that have not undergone peer review.
They should not be considered conclusive, used to inform clinical practice,
or referenced by the media as validated information.

Thickness and Field-dependent evolution ofmagnetic domains in ferrimagnetic TbFe thin films

Keerthana P
Indian Institute of Technology Hyderabad
Saroj Kumar Mishra
Indian Institute of Technology Hyderabad
Jyoti Ranjan Mohanty
jmohanty@phy.iith.ac.in

Indian Institute of Technology Hyderabad

Research Article

Keywords:

Posted Date: November 13th, 2026

DOI: https://doi.org/10.21203/rs.3.rs-11510124/v1

License: This work is licensed under a Creative Commons Attribution 4.0 International License.
Read Full License

Additional Declarations: No competing interests reported.

Thickness and Field-dependent evolution of magnetic domains in ferrimagnetic TbFe thin films

Keerthana P[1], Saroj Kumar Mishra[1], Jyoti Ranjan Mohanty[1*]

[1*]Nanomagnetism and Microscopy Laboratory, Department of Physics, Indian Institute of Technology Hyderabad, Kandi, Sangareddy, 502285, Telangana, India.

*Corresponding author(s). E-mail(s): jmohanty@phy.iith.ac.in;
Contributing authors: ph23resch11010@iith.ac.in;
ph21resch11013@iith.ac.in;

Abstract

Rare-earth–transition-metal ferrimagnetic thin films have emerged as a versatile material platform for spintronic and magnetic memory technologies, owing to their rich magnetic domain behavior and the ability to engineer perpendicular magnetic anisotropy (PMA). Although magnetic reversal and domain dynamics can be tailored through multilayer architectures and interface modification, the extent to which film thickness alone can modulate domain evolution and magnetization-reversal pathways in single-layer ferrimagnets remains insufficiently explored. In this work, we examine the combined influence of film thickness and an externally applied out-of-plane (OOP) magnetic field on the domain dynamics and magnetization reversal mechanisms of single-layer TbFe ferrimagnetic films. TbFe films of 30 and 100 nm thicknesses were deposited by electron-beam evaporation and systematically characterized using vibrating-sample magnetometry (VSM) and magnetic force microscopy (MFM). Magnetometry measurements revealed strong PMA in both samples, accompanied by wasp-waisted OOP hysteresis loops, characteristic of exchange-coupled magnetic sublattices. MFM revealed labyrinthine domain patterns in both films. Upon the application of positive OOP magnetic field, both films undergo complete magnetization reversal, where switching dynamics differ markedly. The 30 nm film exhibits an abrupt reversal accompanied by a narrow and symmetric switching-field distribution, whereas the 100 nm film reverses gradually through viscous domains and with broader switching-field distribution. Field-dependent domain imaging further shows distinct and asymmetric domain-evolution pathways, consistent with a Kondorsky-type reversal mechanism. XPS depth profiling of film revealed pronounced compositional inhomogeneity and Fe/Tb imbalance, directly

linking chemical inhomogeneity, defect-mediated pinning, and sublattice-specific anisotropy that govern the observed reversal asymmetry. These results highlight the combined effects of film thickness and external magnetic fields on TbFe domain dynamics, guiding the design of single-layer ferrimagnetic thin films with precise domain control and reversible switching for memory and spintronic applications.

Keywords: Ferrimagnetic thin films Perpendicular magnetic anisotropy Magnetic domain imaging Field evolution of domains Domain reversal.

1 Introduction

Rare-earth–transition-metal (RE–TM) ferrimagnetic (FiM) alloys constitute a technologically important class of materials, in which localized 4f moments of rare-earth ions are antiferromagnetically coupled to itinerant 3d moments of transition metals, giving rise to two oppositely aligned magnetic sub-lattices with unequal magnetizations [1–6]. This ferrimagnetic configuration yields tunable net magnetization along with large uniaxial magnetic anisotropy, giant magnetostriction, and well-defined compensation phenomena, allowing precise tailoring of the magnetic response by tuning temperature, composition, film thickness, and applied magnetic field [7–12]. As a result, RE–TM ferrimagnets are extensively explored in high-sensitivity magnetic sensors, actuators, transducers, microelectromechanical systems (MEMS), high-density magnetic recording media, energy-harvesting elements, and a broad range of spintronic device concepts [13–18]. Within the broader RE–TM family, thin-film ferrimagnets such as TbFe [19–21], TbFeCo [22–24], GdFe [25–27], and GdCo [28, 29] are particularly attractive for spintronic applications, as they combine antiferromagnet-like ultrafast spin dynamics with a finite net magnetization which allows efficient electrical readout and compatibility with conventional read–write architectures [30–32]. These amorphous ferrimagnetic alloys exhibit robust perpendicular magnetic anisotropy(PMA), strong domain-wall pinning, and composition-dependent magnetic compensation points, which enable applications in high-density non-volatile memories, spin-transfer- and spin-orbit-torque-driven switching, high-velocity domain-wall and skyrmion motion, and all-optical helicity-dependent magnetization reversal [33–36]. By tuning the composition of RE and TM elements, adjusting layer thickness, and tailoring interfacial structures, the magnetic properties of RE–TM ferrimagnetic thin films can be precisely engineered. These tunable characteristics make them essential material platforms for racetrack memory, magneto-optical recording, and other CMOS spintronic technologies [37–39].

Terbium–iron (TbFe) alloys are distinguished among RE–TM ferrimagnets due to their strong spin–orbit coupling originating from the electronic configuration of the Tb ion, whose 4f states lie a few electronvolts below the Fermi level and interact efficiently with visible light, leading to a strong magneto-optical response [40–43]. This strong spin–orbit coupling, together with the amorphous structure, enables TbFe

alloys to possess large PMA, a tunable compensation temperature near room temperature, and local sperimagnetic configurations, which are advantageous for ultrafast magnetic switching and opto-magnetic applications. From a spintronics perspective, TbFe alloys combine strong PMA with relatively low net magnetization, causing narrow, strongly pinned domain walls that are highly responsive to spin-transfer and spin–orbit torques [44–46]. Experiments on TbFe wires with PMA have demonstrated highly efficient domain-wall motion driven by both electric current and magnetic fields. The domain walls move much faster than in conventional ferromagnets, and their behavior changes significantly near the compensation point, where the dynamics are governed by angular-momentum-compensated ferrimagnetic effects [47–49]. Along with the ability to control domain configurations in TbFe structures using voltage and strain, these characteristics position TbFe as an excellent model system for advanced spintronic applications. In particular, it is well suited for domain-wall and skyrmion-based logic, neuromorphic components, and other high-speed devices that demand precise and energy-efficient control of magnetic textures [50–52].

Previous studies have explored individual aspects of TbFe-based ferrimagnetic films, including thickness, magnetic anisotropy, compensation behavior, and field-driven dynamics. In amorphous TbFe thin films, the compensation point, remanent magnetization, and magnetic anisotropy depend on both composition and thickness, evolving up to a critical thickness of 20–30 nm and efficient all-optical switching is further favored in films with low remanent magnetization [53]. Basumatary et al. showed that increasing the thickness of amorphous TbFe thin films promotes the formation of a nano-columnar microstructure and strong PMA, with thickness-induced microstructural changes directly reflected in the domain morphology and magnetic anisotropy [54]. Studies on amorphous TbFeCo thin films have revealed thickness-dependent shifts in the compensation temperature. Depth-resolved magnetic measurements, supported by Monte Carlo simulations, attribute these shifts primarily to interfacial effects, highlighting the critical role of substrate and interface engineering in ultra-thin ferrimagnetic films for spintronic applications [55].

Further insights into related TbFe–based systems and their dynamics underscore the broader relevance of Tb-containing ferrimagnets. Gorbunov et al. showed that $TbFe_5Al_7$ single crystals undergo spontaneous and field-induced spin-reorientation transitions with strong magnetoelastic coupling, revealing multiple magnetic phases and the complex interplay of anisotropy and exchange interactions in rare-earth intermetallic ferrimagnets [56]. Domain-wall motion in TbFe nanowires with perpendicular anisotropy can be efficiently driven by spin-transfer torque and Joule heating, with the enhanced efficiency attributed to the internal domain-wall structure and low net magnetization characteristic of ferrimagnets [57]. Together, these studies establish that composition, thickness, and field history jointly govern compensation behavior, anisotropy, and domain dynamics in TbFe systems.

Although previous studies have separately examined the thickness-dependent magnetic properties of TbFe ferrimagnetic materials and the field-dependent evolution in various ferrimagnets, a comprehensive analysis integrating both thickness and magnetic field effects on domain evolution in single-layer TbFe systems remains lacking.

In the present work, we address this gap by systematically investigating the simultaneous influence of film thickness and an externally applied magnetic field on the domain structure and magnetization reversal processes in an amorphous TbFe single-layer, without relying on multilayer stacks or interface engineering. TbFe films with thicknesses of 30 and 100 nm were deposited at a growth rate of 1.4 Å/s by electron-beam evaporation, and magnetization measurements revealed strong PMA together with a wasp-waisted hysteresis loop, characteristic of exchange-coupled magnetic subsystems with different switching fields. Using magnetic force microscopy (MFM), a detailed analysis of domain morphology and its evolution under varying magnetic field strengths was performed for both film thicknesses. Correlating the MFM images with the magnetization data provides new insight into the mechanisms governing domain evolution under external out-of-plane (OOP) magnetic fields. These results enhance our understanding of how film thickness and an externally applied magnetic field jointly govern domain evolution and magnetization reversal in RE-TM ferrimagnets, and outline strategies for designing spintronic and magneto-optical devices that require controlled domain manipulation.

2 Experimental details

Thin films of TbFe with thicknesses of 30 and 100 nm were deposited onto Si(100) substrates at room temperature using an electron-beam evaporation technique. Prior to deposition, the vacuum chamber was evacuated to a base pressure of 1 $\times 10^{-7}$ mbar to ensure a clean growth environment. Film deposition was carried out using an alloy target with an equiatomic Tb–Fe composition, and the growth rate was tuned to 1.4 Å/s. A protective capping layer of 3 nm chromium (Cr) was deposited on top of the magnetic layers to prevent oxidation. The growth rate and film thickness were monitored and regulated using a quartz crystal microbalance. The substrate was rotated at 20 rpm during deposition to ensure uniform deposition. The film thickness and surface morphology, including roughness measurements, were characterized by atomic force microscopy (AFM). Elemental analysis was performed using energy-dispersive X-ray spectroscopy (EDS) to verify and quantify the atomic ratios of Tb and Fe in the films. Magnetic properties were investigated through hysteresis measurements conducted in both in-plane and out-of-plane geometries using a vibrating sample magnetometer (VSM) (Lakeshore 8607). The evolution of the magnetic domain structures was imaged by MFM (Park NX10 system). An external magnetic field perpendicular to the film plane was applied using a digitally controlled magnetic field generator (MFG, CAYLAR) integrated into the characterisation setup, enabling a systematic study of field-dependent domain behaviour. Depth-resolved chemical analysis was performed by X-ray photoelectron spectroscopy (XPS) using a monochromatic Al-Kα X-ray source (1486 eV) in an AXIS Supra system (Kratos Analytical), in order to probe compositional inhomogeneities and sublattice imbalance across the TbFe film.

3 Results and discussions

The field-magnetization (M–H) response of the TbFe films was measured in both in-plane (IP) and out-of-plane (OOP) directions. Both 30 nm and 100 nm TbFe

films exhibit nearly identical OOP hysteresis loops characterized by a double-step approach to saturation rather than a single rectangular loop, indicating a two-stage magnetization reversal process. This "wasp-waisted" loop shape is characteristic of systems containing exchange-coupled magnetic subsystems with different switching fields. This is commonly associated with coexisting hard and soft regions, as locally observed in Tb-rich and Fe-rich environments within a single-phase ferrimagnet. In amorphous TbFe, this behavior is naturally linked to hard and soft regions, such as slightly Tb-rich and Fe-rich environments, and to the different anisotropies of the Tb and Fe sublattices, so that the magnetically soft part of the film reverses at relatively low fields and the remaining harder regions only switch at higher fields, giving an exchange-coupled-like double saturation without requiring a separate antiferromagnetic layer [58–60].

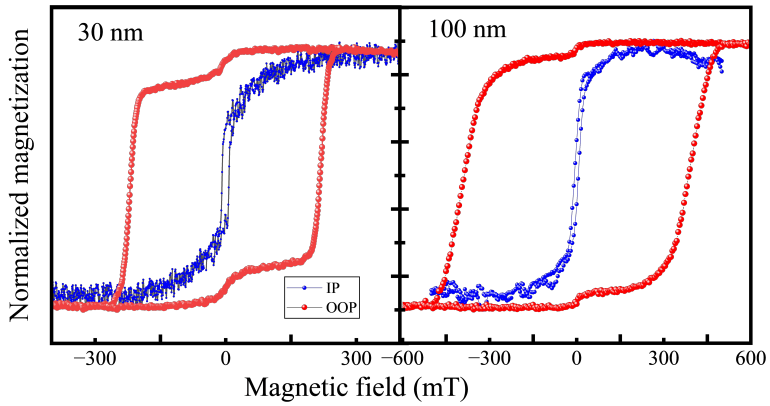


Fig. 1 Normalized magnetization as a function of the applied magnetic field for TbFe films with thicknesses of 30 nm and 100 nm, measured in both in-plane and out-of-plane directions.

Figure 1 presents the IP and OOP M-H loops of 30 and 100 nm TbFe films. The OOP M-H loops show distinct saturation at approximately 300 mT for the 30 nm film and 500 mT for the 100 nm film, indicating strong PMA. Analysis of the coercive field (H_c) values reveals 9 mT and 6 mT in the IP direction for 30 nm and 100 nm films, respectively, while in the OOP direction, the (H_c) increases markedly from 217 mT in the 30 nm film to 384.4 mT in the 100 nm film, indicating a pronounced enhancement of (H_c) with increasing thickness in the OOP orientation. The increased (H_c) observed in the 100 nm film can be associated with the evolution of strongly pinned magnetic domains with increasing thickness. Such domain configurations hinder domain wall motion, thereby enhancing the resistance to magnetization reversal.

The elemental composition of both TbFe films was quantified by energy dispersive X-ray spectroscopy (EDS) coupled to a field emission scanning electron microscope (FESEM), as presented in Table 1. The 30 nm and 100 nm samples exhibit nearly identical stoichiometries of $Tb_{17.6}Fe_{82.4}$ and $Tb_{17.8}Fe_{82.2}$, respectively, indicating that within the experimental uncertainty, both films can be regarded as compositionally

equivalent and lie on the Fe-rich side of the Tb–Fe phase space. In both cases, the Fe concentration is significantly higher than that of the nominal $Tb_{50}Fe_{50}$ target alloy, consistent with the commonly reported preferential incorporation of Fe during deposition of amorphous TbFe thin films [53, 54]. This behaviour can be explained by the higher vapour pressure of Fe relative to Tb near the alloy melting temperature of 1500 K [61]. At 1600 K, the vapour pressures of Fe and Tb have been reported as 9.61 $\times 10^{-1}$ Pa and 5.85 $\times 10^{-2}$ Pa, respectively [62]. At a particular temperature, the element with the higher vapour pressure evaporates more readily than the one with the lower vapour pressure, leading to a higher concentration of that element in the atomic flux arriving at the substrate and, consequently, in the deposited film.

Table 1 Estimated parameters such as stoichiometry, rms roughness (R_q),domain width (λ), uniaxial anisotropy (K_u), Coercivity (H_c), Spontaneous magnetization (M_s).

Film thickness (nm)	Stoichiometry (atomic %)	R_q (nm)	λ (nm)	K_u ($\times 10^5 J/m^3$)	H_c (mT)	M_s (kA/m)
30	$Tb_{17.6}Fe_{82.4}$	0.15	307($\pm$38)	0.4	216.7	185
100	$Tb_{17.8}Fe_{82.2}$	0.33	322($\pm$31)	0.43	384.4	186

The microscopic analysis of the 30 and 100 nm films are shown in figure **??**, and the corresponding root-mean-square roughness (R_q) extracted from AFM measurements is listed in table 1. The AFM images of 30 and 100 nm showed that the value of the (R_q) is less than 1 nm, indicating that the film surfaces are very smooth with a uniform, continuous morphology and minimal height fluctuations. MFM measurements were conducted after the samples were demagnetized using an OOP magnetic field of strength 600 mT. Both films exhibit characteristic labyrinth-like domain patterns with high magnetic phase contrasts. To reduce topographic artifacts in the magnetic phase signal, arising from the combined influence of short-range van der Waals forces and long-range magnetic interactions, the measurements were conducted at a constant lift height of 20 nm. The quantitative analysis of the domain patterns was performed using the two-dimensional Fourier transform (2D-FFT) of the MFM images. The corresponding isotropic power spectral density (PSD) profiles, shown in Figure 2(c), provide the characteristic domain periodicity. The peak in the PSD curve, obtained through Lorentzian fitting, corresponds to the inverse of the periodicity, while half of this value defines the domain size (λ). The associated error bars are derived from the full width at half maximum (FWHM) of the fit. Table 1 lists the extracted domain sizes for each film thickness. The circular FFT maps (insets of Fig.3c) confirm that the domains are isotropically distributed, with no preferred orientation, consistent with the complex morphology observed in the two films.

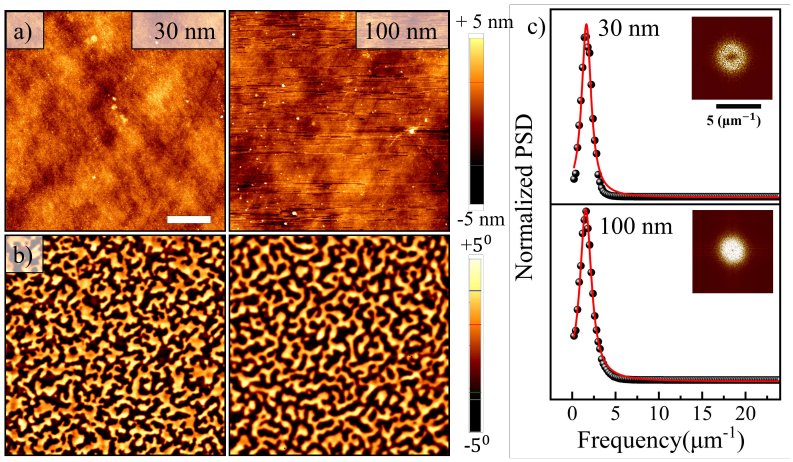


Fig. 2 Normalized (a) AFM, (b) MFM images after demagnetization for TbFe films of varying thickness, and the corresponding thickness values are indicated in the top right corner of AFM images. A consistent scale bar of 2 µm is maintained across all the images, and c)The 2D isotropic power spectral density profile, along with the corresponding 2D-FFT pattern of the MFM images, is shown as insets for 30 and 100 nm TbFe films.

Field-dependent MFM measurements were performed to understand the magnetic domains evolution in both films. An external OOP magnetic field, up to a maximum of 200 mT, was applied to the 30 nm and 100 nm TbFe films using a calibrated MFG. The corresponding changes in domain structure at different field strengths were then imaged by MFM. Upon applying the field to a specific threshold value, magnetization reversal of the domains was observed, transitioning from up to down magnetization. This phenomenon remained consistent across repeated measurements, with both film thicknesses exhibiting reliable, reproducible full-domain switching. As the field was further increased, the magnetic domains successively fragmented and coalesced, leading to the formation of a single-domain state aligned with the external field. These results demonstrate the strong PMA and uniform switching behavior of TbFe films, and provide insight into the domain dynamics as a function of applied field and film thickness.

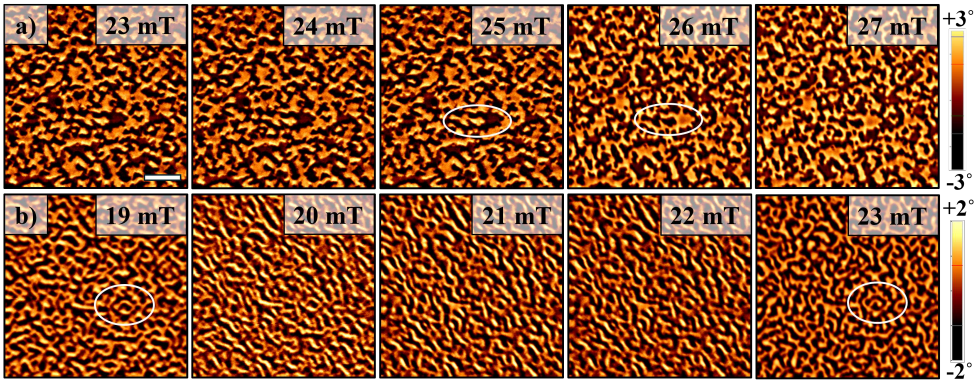


Fig. 3 MFM images showing domain reversal as a function of applied OOP magnetic field for TbFe films of thickness (a) 30 nm and (b) 100 nm. The corresponding field values are indicated in the upper right corner of each image; the inset circles in a and b highlight representative regions where the local domain reversal has occurred. and all MFM images share a common scale bar of 1 µm.

For the 30 nm film, the application of an external magnetic field resulted in abrupt, complete domain reversal at a single critical field. In contrast, the 100 nm film displayed a more complex reversal process: domains entered a viscous, metastable state and continued to evolve over a range of applied fields before achieving full reversal. Domain reversal was examined in detail by taking MFM images at 1 mT field intervals for both the 30 and 100 nm TbFe films, as shown in fig. 3. In the 30 nm film, the domain pattern remained unchanged up to 25 mT, then switched completely at 26 mT, indicating an abrupt, all-at-once reversal rather than a gradual nucleation process. The 100 nm film, however, behaved differently: once the field exceeded 19 mT, the domains entered a viscous metastable state at 20 mT, which persisted up to 22 mT; only at 23 mT did the magnetization fully reverse. This difference arises from the increased density and strength of domain-wall pinning centers in thicker films, which hinder domain-wall motion and give rise to a multi-step reversal mechanism. As film thickness increases, the domain structure becomes progressively more complex, and intermediate domain states are stabilized over a broader field range, indicating increased coercivity and pinning effects.

To understand the differences in magnetization reversal mechanisms between the 30 nm and 100 nm films, the switching field distributions (dM/dH) of both samples were systematically analyzed and compared. From fig. 4, the dM/dH reveals distinct reversal pathways in the two films. The 30 nm film exhibits highly symmetrical and sharply peaked profiles for both magnetization branches, characteristic of an abrupt reversal process. In this regime, magnetization switching occurs collectively through coherent domain wall motion, where strong PMA stabilizes domains and promotes rapid propagation once nucleation is triggered. In contrast, the 100 nm film displays a noticeably broader distribution, indicative of a viscous reversal mechanism. Here, magnetization changes progressively as the applied field is swept, with local variations in microstructure and compositional inhomogeneity introducing a spread of switching

fields. Domain walls encounter pinning centers such as defects, grain boundaries, or thickness-induced irregularities, which hinder their motion and force partial rotation of magnetic moments before complete reversal occurs. This defect-mediated process can produce broadened profiles, highlighting the gradual, non-coherent nature of viscous reversal [63]. The broadening of the switching field distribution is further consistent with inter-granular dipolar interactions, wherein stray fields from neighboring grains introduce local variations in the effective switching field and stabilize intermediate domain states, thereby promoting a viscous, non-coherent reversal process. Together, these contrasting behaviors emphasize that abrupt reversal arises when anisotropy-driven domain wall motion dominates, while viscous reversal emerges when pinning and microstructural disorder govern the dynamics. The transition observed between the 30 nm and 100 nm TbFe films thus reflects the evolving interplay between film microstructure, domain dynamics, and magnetization reversal processes as a function of thickness [64, 65].

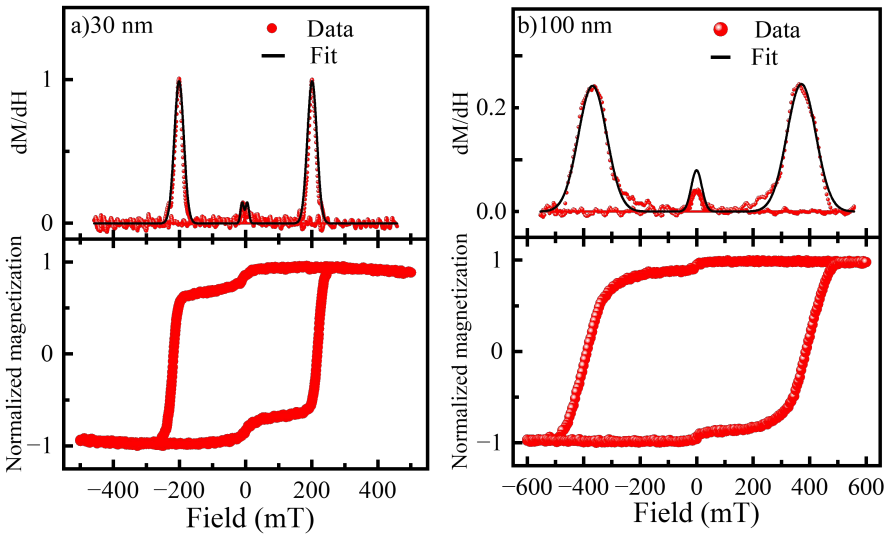


Fig. 4 The switching-field distributions dM/dH and the corresponding magnetic hysteresis loops of TbFe films with thicknesses of (a) 30 nm and (b) 100 nm. The dot symbols denote the experimental data, and the solid lines represent the fitted integrated switching-field distributions.

Figure 5 illustrates the evolution of up magnetization and down magnetization in the 30 nm TbFe film as a function of the applied OOP magnetic field. At low magnetic fields, the film predominantly exhibits up magnetization, with down magnetization remaining limited. Notably, a rapid and complete reversal of magnetic domains occurs between the fields 20 mT and 30 mT, with the up magnetization abruptly decreasing and the down magnetization increasing correspondingly. Including representative domain images in the graph provides clear visual evidence of this transition, showing the film's complete shift from an up magnetization to a down magnetization within this field window. With further increase in the field, the sample approaches magnetic

saturation, where down magnetization dominates nearly the entire region. These findings highlight the sharp, efficient switching behavior of the TbFe film, signifying its strong PMA and highly mobile domain walls in response to applied external magnetic fields.

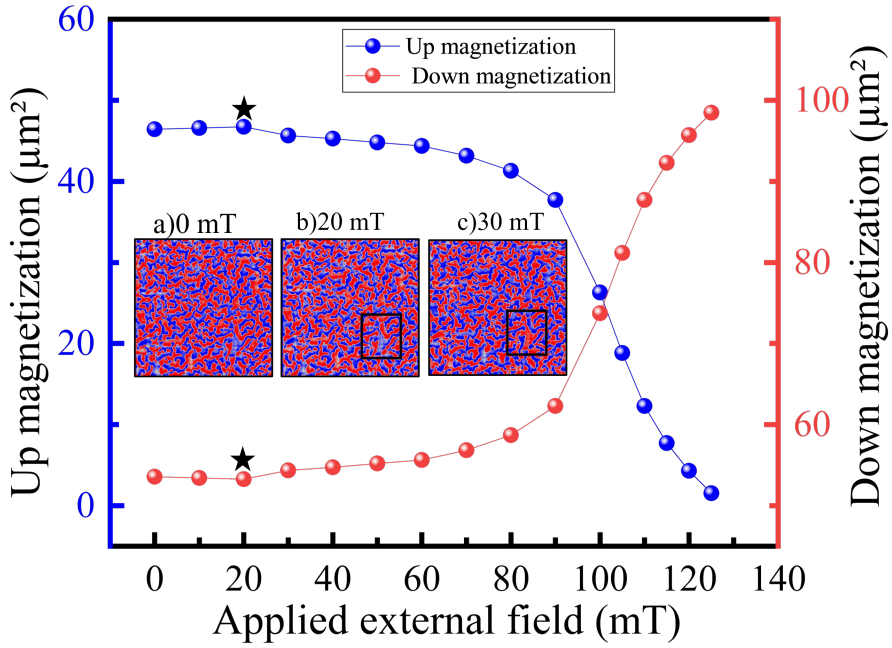


Fig. 5 Evolution of spin-up and spin-down domain areas in the 30 nm TbFe film under increasing positive out-of-plane magnetic field. Stars indicate the characteristic field values corresponding to reversal onset for each polarity. Domain images correspond to applied fields of (a) 0 mT, (b) 20 mT, and (c) 30 mT. At 20 and 30 mT, nearly complete reversal of the labyrinth domains is observed; The inset boxes in (b) and (c) highlight representative regions where the local domain reversal has occurred.

Upon examining the magnetization reversal in TbFe thin films under positive and negative OOP magnetic fields, we observed distinct domain behaviors. In a positive OOP field, the domains undergo complete magnetization reversal at a specific field value; upon further increasing the field, the reversed domains fragment and then gradually reach a stable single-domain state. In contrast, when a negative OOP field is applied, there is no analogous one-step reversal at a specific field; instead, the domains progressively become unstable and fragmented with increasing field strength, and gradually settle into a single domain. Figure 6 illustrates magnetic domain images acquired under positive and negative magnetic fields at various field strengths in different regions of the 30 nm film. A clear asymmetry in domain evolution is observed. Rather than following the ideal, symmetric coherent rotation predicted by the Stoner–Wohlfarth model, the films exhibit behavior more consistent with a Kondorsky-type mechanism, in which domain-wall motion and pinning dominate the

switching process [67]. Here, in this case, defects and microstructural inhomogeneities can act as pinning sites, making reversal easier for one field polarity and more strongly hindered for the opposite field polarity. The resulting direction-dependent asymmetry suggests that the pinning centers and intrinsic anisotropy within the film play a key role in determining the magnetization-reversal pathway.

The asymmetry in magnetization reversal between positive and negative field polarities can be understood in terms of nucleation density. When a positive magnetic field is applied, numerous nucleation sites form across the film, providing multiple centers for reversed domains to initiate and expand. The high density of nucleation points facilitates complete domain reversal as these domains grow and coalesce, though saturation is achieved only at relatively higher fields, around +140 mT, due to the need to overcome pinning and drive domain wall motion. In contrast, under negative field polarity, nucleation sites are fewer, limiting the initiation of reversed domains. As a result, no large-scale domain reversal is observed, and the magnetization aligns more directly with the applied field, leading to saturation at a lower field of approximately –120 mT. This polarity-dependent difference is clearly demonstrated in the MFM images presented in Figure 6, which highlight the contrasting nucleation behavior.

Here, in an applied field of 140 mT, the smallest domain size mapped from the MFM line profile is 137 nm. Beyond this field, the domain features approach the intrinsic resolution limit of the MFM tip, which is determined by the probe radius and coating thickness, the convolution of the tip stray field with the sample stray field, the tip–sample lift height, and the stability of the tip magnetization [68]. Under these conditions, reliable imaging is typically restricted to features larger than 130 nm, and as domains shrink below this threshold, the tip response becomes broadened, reducing quantitative accuracy. The application of an external OOP magnetic field further complicates resolution by modifying the tip magnetization state and altering its effective stray field profile, while simultaneously driving domain wall motion, nucleation, and fragmentation within the sample. These coupled effects make fine domain structures increasingly difficult to resolve, and the domains progressively coalesce until the film approaches magnetic saturation.

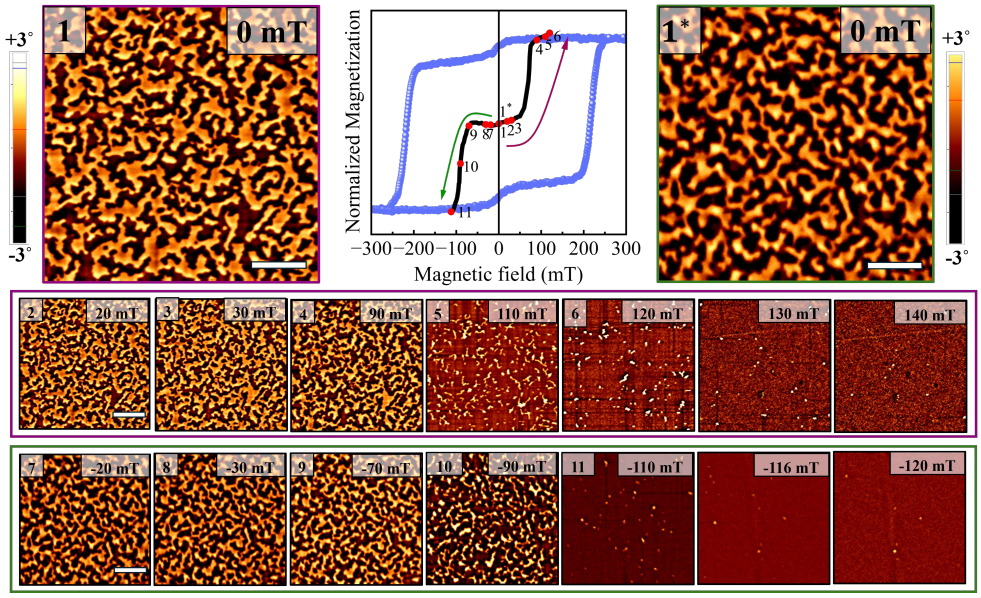


Fig. 6 OOP hysteresis loop of the 30 nm TbFe film and the black line traces the magnetic field sweep used during MFM imaging of the demagnetized sample, with discrete points labeled 1-11 denoting the applied OOP magnetic field values. The zero-field MFM images shown adjacent to the loop were recorded at different spatial positions of the sample during measurements, with the left-side image corresponding to the positive-field sequence and the right-side image to the negative-field sequence. Below the loop, the sequence of MFM images illustrates domain evolution under increasing positive and negative external magnetic fields. The specific field value is indicated in the upper right corner of each image. All images share a common scale bar of 1 µm across the full set of field values.

XPS depth profiling was performed to probe the microscopic origin of reversal asymmetry in the 30-nm TbFe film. The sample was sequentially etched for 300 s, 420 s, and 480 s, and wide spectra were collected at each stage. Fig.7a shows the XPS wide spectra for the 30 nm TbFe spectra (black) and spectra collected after etching for 300 s (red), 420 s (blue) and 480 s (green), highlighting the evolution of Fe and Tb films with depth. The relative contribution of each element was quantified by analyzing the peak area of fitting the Shirley background corrected fine scans of XPS spectra for Fe (core-shell) and Tb (core-level) using CasaXPS [REF] software [69].

The time-dependent variation in the peak areas of Tb and Fe is shown in Figure 7b, revealing a clear chemical imbalance across the 30 nm TbFe film: the Fe signal diminishes rapidly with depth, while Tb intensity rises and eventually stabilizes [70]. This non-uniform distribution indicates chemical inhomogeneity within the stack, which naturally introduces defects and local anisotropy variations. Such irregularities act as pinning centers, shaping how domains nucleate and propagate under an applied field.

When the field is applied in the positive polarity, reversal proceeds through Fe-rich regions. The Fe sublattice, with its relatively weak spin–orbit coupling (SOC), presents a lower exchange threshold. Within the Elliott–Yafet framework, conduction electrons

in Fe experience only modest spin–orbit mixing, which increases the likelihood of spin-flip scattering events [71]. These spin flips reduce the energetic barrier for domain nucleation, allowing many nucleation sites to form and enabling complete reversal across the film [72].

In contrast, under negative polarity, the reversal pathway is forced through Tb-rich regions. The Tb sublattice is dominated by strong SOC; this coupling reduces the flexibility of spin states and raises the energetic threshold for spin reorientation [73, 74]. In the EY picture, this strong SOC suppresses spin flip scattering because spin states are more rigidly locked, raising the exchange threshold required for reversal. As a result, nucleation is sparse, domain walls encounter stronger pinning, and reversal remains incomplete [75]. Thus, the observed asymmetry in magnetization reversal is not simply a magnetic artifact but emerges from the interplay between chemical inhomogeneity (Fe/Tb imbalance), defect-mediated pinning centers, and the intrinsic sublattice-dependent SOC captured by the Elliott–Yafet mechanism. Together, these factors define the reversal pathway and explain why one field polarity supports abundant nucleation and full reversal, while the opposite polarity is hindered.

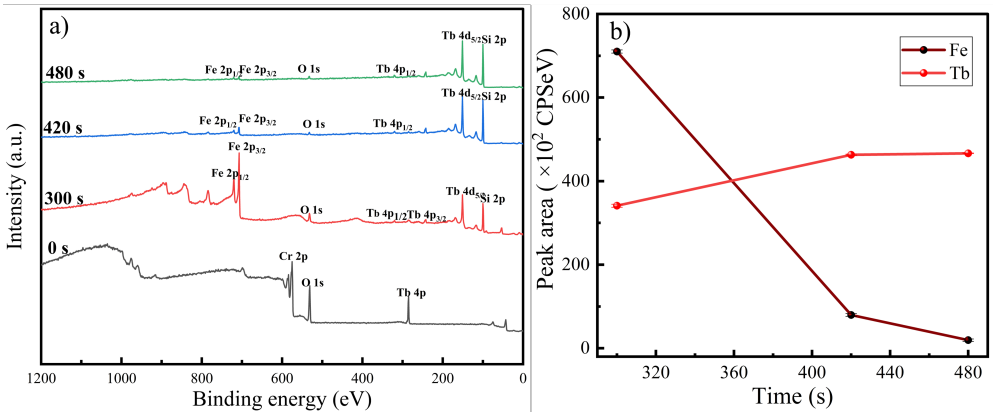


Fig. 7 (a) Wide XPS spectra of the TbFe film before etching and after 300 s and 480 s etching. (b) Variation of Tb and Fe peak areas with etching time (300 s, 420 s, and 480 s), obtained from high-resolution spectra using CasaXPS with Shirley-background subtraction.

4 Conclusion

We systematically studied the effect of thickness and magnetic field on domain evolution and magnetization reversal in single-layer TbFe thin films deposited by the electron-beam evaporation technique. M–H measurements showed strong PMA with wasp-waisted OOP hysteresis loops. EDS analysis confirmed nearly identical stoichiometries for both TbFe films. Films showed labyrinth-like domain patterns after demagnetization. The domain evolution of both films was examined by applying positive and negative OOP magnetic fields. Under the positive OOP field, both films showed complete magnetization reversal. The 30 nm film reversed abruptly with a

narrow, symmetric switching-field distribution, whereas the 100 nm film reversed gradually through a viscous metastable domain state, with a broader distribution. Under both positive and negative OOP magnetic fields, films showed distinct, asymmetric domain evolution, with reversal behavior consistent with the Kondorsky model. XPS depth profiling establishes that compositional inhomogeneity and Fe/Tb imbalance across the TbFe film introduce defect-mediated pinning and sublattice-specific anisotropy, thereby providing a microscopic basis for the observed reversal asymmetry. These results show that tuning thickness and application of magnetic field in TbFe single layers enable precise control of PMA, domain behavior, and magnetization reversal, facilitating their application in spintronic and memory devices where precise domain control and reversible switching are essential.

Acknowledgements. K.P. acknowledges IIT Hyderabad for providing research facilities. J.R.M. acknowledges the funding support from DST Nanomission (project no. DST/NM/TUE/QM-4/2019-IIT-H). Also, we acknowledge the DST - FIST facility, VSM at the Department of Physics, IIT Hyderabad (Project No: SR/FST/PSI-215/2016).

Author contributions. **Keerthana P:** Conceptualization, Investigation, Formal analysis, Methodology, Writing - original draft, Writing—review and editing. **Saroj Kumar Mishra:** Methodology, Writing - Review, Editing. **Jyoti Ranjan Mohanty:** Conceptualization, Investigation, Methodology, Writing - review

Data availability. The data that support the results of this study are available from the corresponding author upon reasonable request.

Declarations

Conflict of interest The authors have no financial or commercial conflict to disclose.

References

[1] Mimura, Y., Imamura, N. and Kushiro, Y., 1976. Hall effect in rare-earth–transition-metal amorphous alloy films. J. Appl. Phys., 47(7), pp.3371-3373.

[2] Mansuripur, M. and Ruane, M., 2003. Mean-field analysis of amorphous rare earth-transition metal alloys for thermomagnetic recording. IEEE Trans. Magn., 22(1), pp.33-43.

[3] Talapatra, A., Umadevi, K., Chelvane, J.A., Mohanty, J. and Jayalakshmi, V., 2018. Magnetic domains in Tb-Fe-Co thin films under anisotropy tilt. J. Magn. Magn. Mater., 452, pp.108-113.

[4] Kee, J.Y., Kim, K.T., Lee, I.H., Seo, I., Chang, J.Y., Lee, A.Y., Noh, W.S., Chang, Y.J., Park, S.Y., Choe, S.B. and Kim, D.H., 2024. Additive roles of antiferromagnetically coupled elements in the magnetic proximity effect in the GdFeCo/Pt system. Sci. Rep., 14(1), p.9476.

[5] Gschneidner, K.A., Bunzli, J.C.G. and Pecharsky, V.K., 2004. Handb. Phys. Chem. Rare Earths (Vol. 34). Elsevier.

[6] Jensen, J. and Mackintosh, A.R., 1991. Rare Earth Magnetism: Rare earth magnetism: structures and excitations. Oxford Univ. Press.

[7] Bessais, L., 2021. Structure and magnetic properties of intermetallic rare-earth-transition-metal compounds: a review. Materials, 15(1), p.201.

[8] Jha, A.R., 2014. Rare earth materials: properties and applications. CRC Press.

[9] Sarkis, A. and Callen, E., 1982. Magnetic anisotropy of rare-earth—transition-metal compounds. Phys. Rev. B, 26(7), p.3870.

[10] Quandt, E., 1997. Giant magnetostrictive thin film materials and applications. J. Alloys Compd., 258(1-2), pp.126-132.

[11] Ghanathe, M., Kumar, A. and Yusuf, S.M., 2019. Microscopic and mesoscopic understanding of magnetization compensation phenomenon in ferrimagnetic Li0. 5FeCr1. 5O4 spinel. J. Appl. Phys., 125(9).

[12] Donges, A., Khmelevskyi, S., Deak, A., Abrudan, R.M., Schmitz, D., Radu, I., Radu, F., Szunyogh, L. and Nowak, U., 2017. Magnetization compensation and spin reorientation transition in ferrimagnetic DyCo 5: Multiscale modeling and element-specific measurements. Phys. Rev. B, 96(2), p.024412.

[13] Quandt, E. and Ludwig, A., 2000. Magnetostrictive actuation in microsystems. Sensors and Actuators A: Physical, 81(1-3), pp.275-280.

[14] Burzo, E., Rare Earth-Transition Metal Compounds: Magnetism and Applications. New Magn. Mater. Their Funct., p.11.

[15] Matizamhuka, W., 2018. The Impact of Magnetic Materials in Renewable Energy-Related Technologies in the 21st Century Industrial Revolution: The Case of South Africa. Adv. Mater. Sci. Eng., 2018(1), p.3149412.

[16] Gupta, S., 2023. Exotic rare earth-based materials for emerging spintronic technology. Handb. Phys. Chem. Rare Earths, 63, pp.99-140.

[17] Gao, C., Zeng, Z., Peng, S. and Shuai, C., Magnetostrictive alloys: promising materials for biomedical applications. Bioact Mater 2022; 8: 177–95 [online]

[18] Gibbs, M.R.J., Hill, E.W. and Wright, P.J.E.W., 2007. Chapter Six Magnetic Microelectromechanical Systems: MagMEMS. Handb. Magn. Mater., 17, pp.457-526.

[19] Sahoo, A.K., Chelvane, J.A. and Mohanty, J., 2023. High coercive field in TbFe/Fe/TbFe exchange-coupled system with mixed magnetic anisotropy. Appl.

Phys. A, 129(6), p.419.

[20] Sobieszczyk, P. and Krupinski, M., 2024. Surface effects in ferrimagnetic TbFe rare-earth–transition-metal thin films and nanoparticles. Phys. Rev. B, 109(2), p.024412.

[21] Tang, M., Zhang, Z., Zhu, Y., Ma, B. and Jin, Q., 2014. Role of TbFe on perpendicular magnetic anisotropy and giant magnetoresistance effect in [Co/Ni] N-based spin valves. Nano-Micro Lett., 6(4), pp.359-364.

[22] Talapatra, A., Chelvane, J.A. and Mohanty, J., 2021. Engineering perpendicular magnetic anisotropy in Tb-Fe-Co thin films using ion-beam irradiation. J. Alloys Compd., 861, p.157953.

[23] Yuzuak, G.D., Yuzuak, E., Ennen, I. and Hutten, A., 2021. Thickness induced magnetic anisotropic properties of Tb-Fe-Co thin films. Curr. Appl. Phys., 29, pp.33-38.

[24] Liu, T.M., Wang, T., Reid, A.H., Savoini, M., Wu, X., Koene, B., Granitzka, P., Graves, C.E., Higley, D.J., Chen, Z., and Razinskas, G., 2015. Nanoscale confinement of all-optical magnetic switching in TbFeCo-competition with nanoscale heterogeneity. Nano Lett., 15(10), pp.6862-6868.

[25] Kumar Mishra, S., Prasanth Perumal, H. and Mohanty, J., 2024. Engineering perpendicular magnetic anisotropy and Dzyaloshinskii–Moriya interaction in Gd–Fe thin films for spintronics applications. J. Appl. Phys., 136(24).

[26] Mishra, S.K., Poddar, N.P., Chelvane, J.A. and Mohanty, J., 2025. Exploring thickness effects on magnetization reversal mechanism and domain state configuration in ferrimagnetic Gd–Fe thin film. J. Mater. Sci.: Mater. Electron., 36(7), p.413.

[27] Hintermayr, J., Ullrich, A. and Albrecht, M., 2021. Structure and magnetic properties of ferrimagnetic [Gd/Fe] n multilayer and GdxFe100− x thin films. AIP Adv., 11(9).

[28] Binder, M., Weber, A., Mosendz, O., Woltersdorf, G., Izquierdo, M., Neudecker, I., Dahn, J.R., Hatchard, T.D., Thiele, J.U., Back, C. and Scheinfein, M.R., 2006. Magnetization dynamics of the ferrimagnet CoGd near the compensation of magnetization and angular momentum. Phys. Rev. B, 74(13), p.134404.

[29] Fu, T., Li, S., Feng, X., Cui, Y., Yao, J., Wang, B., Cao, J., Shi, Z., Xue, D. and Fan, X., 2021. Complex anomalous Hall effect of CoGd alloy near the magnetization compensation temperature. Phys. Rev. B, 103(6), p.064432.

[30] Zhu, K., Bi, L., Zhang, Y., Zheng, D., Yang, D., Li, J., Tian, H., Cai, J., Yang, H., Zhang, Y. and Li, J., 2024. Ultrafast switching to zero-field topological spin

textures in ferrimagnetic TbFeCo films. Nanoscale, 16(6), pp.3133-3143.

[31] Khorsand, A.R., Savoini, M., Kirilyuk, A., Kimel, A.V., Tsukamoto, A., Itoh, A. and Rasing, T., 2013. Element-Specific Probing of Ultrafast Spin Dynamics in Multisublattice Magnets with Visible Light. Phys. Rev. Lett., 110(10), p.107205.

[32] Davies, C.S., Mentink, J.H., Kimel, A.V., Rasing, T. and Kirilyuk, A., 2022. Helicity-independent all-optical switching of magnetization in ferrimagnetic alloys. J. Magn. Magn. Mater., 563, p.169851.

[33] Yuzuak, G.D., 2025. Modifying the magnetic characteristics of ferrimagnetic TbFeCo by adjusting the thickness of the L11-ordered CoPt. J. Alloys Compd., 1020, p.179366.

[34] Ishibashi, M., Yakushiji, K., Kawaguchi, M., Tsukamoto, A., Nakatsuji, S. and Hayashi, M., 2022. Ferrimagnetic compensation and its thickness dependence in TbFeCo alloy thin films. Appl. Phys. Lett., 120(2).

[35] Diona, P., Maranzana, L., Artyukhin, S. and Sala, G., 2025. Observation of relativistic domain wall motion in amorphous ferrimagnets. Adv. Funct. Mater., p.e22549.

[36] van Hees, Y.L., van de Meugheuvel, P., Koopmans, B. and Lavrijsen, R., 2020. Deterministic all-optical magnetization writing facilitated by non-local transfer of spin angular momentum. Nat. Commun., 11(1), p.3835.

[37] Zhang, Y., Feng, X., Zheng, Z., Zhang, Z., Lin, K., Sun, X., Wang, G., Wang, J., Wei, J., Vallobra, P. and He, Y., 2023. Ferrimagnets for spintronic devices: From materials to applications. Appl. Phys. Rev., 10(1).

[38] Suzuki, D.H., 2023. Dzyaloshinskii-Moriya Interaction and Local Exchange Variation in Rare-Earth Transition-Metal Ferrimagnets. MIT.

[39] Rianto, D., Nicholson, B., Hodgkiss, A.W., Caruana, A.J., Kinane, C.J., Bouchenoire, L., Michałowski, P.P., Hase, T.P. and Atkinson, D., 2025. Mapping magnetization orientation within compositionally graded rare-earth transition-metal alloy thin films for spintronics. Commun. Mater., 6(1), p.264.

[40] Zhang, W., Park, J.M., Lee, S.J., Pecharsky, A.O. and Gschneidner Jr, K.A., 2003. Optical and magneto-optical properties of Tb (Mn1− xFex) 2 compounds where x= 0.35, 0.5, 0.65. J. Magn. Magn. Mater., 267(2), pp.197-203.

[41] Thielemann-Kühn, N., Amrhein, T., Bronsch, W., Jana, S., Pontius, N., Engel, R.Y., Miedema, P.S., Legut, D., Carva, K., Atxitia, U. and van Kuiken, B.E., 2024. Optical control of 4 f orbital state in rare-earth metals. Sci. Adv., 10(16), p.eadk9522.

[42] Carey, R., Newman, D.M., Snelling, J.P. and Thomas, B.W.J., 1993. The magnetic and magneto-optical properties of amorphous (TbFeCo) Pr films. J. Magn. Magn. Mater., 128(1-2), pp.204-208.

[43] Shim, J.H., Syed, A.A., Kim, J.I., Piao, H.G., Lee, S.H., Park, S.Y., Choi, Y.S., Lee, K.M., Kim, H.J., Jeong, J.R. and Hong, J.I., 2020. Role of non-thermal electrons in ultrafast spin dynamics of ferromagnetic multilayer. Sci. Rep., 10(1), p.6355

[44] Krupinski, M., Hintermayr, J., Sobieszczyk, P. and Albrecht, M., 2021. Control of magnetic properties in ferrimagnetic GdFe and TbFe thin films by He+ and Ne+ irradiation. Phys. Rev. Mater., 5(2), p.024405.

[45] Chiba, D., Kawaguchi, M., Fukami, S., Ishiwata, N., Shimamura, K., Kobayashi, K.A. and Ono, T., 2012. Electric-field control of magnetic domain-wall velocity in ultrathin cobalt with perpendicular magnetization. Nat. Commun., 3(1), p.888.

[46] Kumar, G.J., Guo, Z., Wang, S., Han, Z. and Wang, K., Influence of Thickness on Magnetic Anisotropy and Magnetocaloric Response in Ta-Capped Rare-Earth Rich Tbfeco Amorphous Thin Films. Available at SSRN 5339708.

[47] Jing, K.Y., Gong, X. and Wang, X.R., 2022. Field-driven domain wall motion in ferrimagnetic nanowires. Phys. Rev. B, 106(17), p.174429.

[48] Siddiqui, S.A., Han, J., Finley, J.T., Ross, C.A. and Liu, L., 2018. Current-induced domain wall motion in a compensated ferrimagnet. Phys. Rev. Lett., 121(5), p.057701.

[49] Haltz, E., Sampaio, J., Krishnia, S., Berges, L., Weil, R. and Mougin, A., 2020. Measurement of the tilt of a moving domain wall shows precession-free dynamics in compensated ferrimagnets. Sci. Rep., 10(1), p.16292.

[50] Hunt, R.G., Moldarev, D., Grassi, M.P., Primetzhofer, D. and Andersson, G., 2025. Control of ferrimagnetic compensation and perpendicular anisotropy in Tb x Co (100_x) with H+ ion implantation. Phys. Rev. Mater., 9(3), p.034409.

[51] Gonzalez Sanz, J.A., Andres González, J.P. and Lopez Antón, R., 2021. Applied Trends in Magnetic Rare Earth/Transition Metal Alloys and Multilayers.

[52] Brock, J.A., Kurenkov, A., Hrabec, A. and Heyderman, L.J., 2025. Engineering and exploiting self-driven domain wall motion in ferrimagnets for neuromorphic computing applications. arXiv:2508.14252.

[53] Hebler, B., Hassdenteufel, A., Reinhardt, P., Karl, H. and Albrecht, M., 2016. Ferrimagnetic Tb–Fe Alloy thin films: composition and thickness dependence of magnetic properties and all-optical switching. Front. Mater., 3, p.8.

[54] Basumatary, H., Chelvane, J.A., Rao, D.S., Talapatra, A., Mohanty, J., Kumar, D., Singh, V., Kamat, S.V. and Ranjan, R., 2021. Understanding thickness-dependent magnetic properties of Tb-Fe thin films. J. Alloys Compd., 869, p.159571.

[55] Ma, C.T., Kirby, B.J., Li, X. and Poon, S.J., 2018. Thickness dependence of ferrimagnetic compensation in amorphous rare-earth transition-metal thin films. Appl. Phys. Lett., 113(17).

[56] Gorbunov, D.I., Yasin, S., Andreev, A.V., Mushnikov, N.V., Skourski, Y., Zherlitsyn, S. and Wosnitza, J., 2014. Spontaneous and field-induced phase transitions in TbFe5Al7. J. Magn. Magn. Mater., 365, pp.56-63.

[57] Haltz, E., Sampaio, J., Weil, R., Dumont, Y. and Mougin, A., 2019. Strong current actions on ferrimagnetic domain walls in the creep regime. Phys. Rev. B, 99(10), p.104413.

[58] Heigl, M., Vogler, C., Mandru, A.O., Zhao, X., Hug, H.J., Suess, D. and Albrecht, M., 2020. Microscopic origin of magnetization reversal in nanoscale exchange-coupled ferri/ferromagnetic bilayers: implications for high energy density permanent magnets and spintronic devices. ACS Appl. Nano Mater., 3(9), pp.9218-9225.

[59] Kharwanlang, R.S. and Shukla, P., 2012. Analysis of wasp-waisted hysteresis loops in magnetic rocks. Phys. Rev. E, 85(1), p.011124.

[60] Bennett, L.H. and Della Torre, E., 2005. Analysis of wasp-waist hysteresis loops. J. Appl. Phys., 97(10).

[61] Dariel, M.P., Holthuis, J.T. and Pickus, M.R., 1976. The terbium-iron phase diagram. J. Less-Common Met., 45(1), pp.91-101.

[62] https://periodic-table.rsc.org/

[63] Perzanowski, M., Zarzycki, A., Gregor-Pawlowski, J. and Marszalek, M., 2020. Magnetization reversal mechanism in exchange-biased spring-like thin-film composite. ACS Appl. Mater. Interfaces, 12(35), pp.39926-39934.

[64] Roman, A., Gomez, J., Butera, A., Vavassori, P. and Steren, L.B., 2024. Magnetization reversal and direct observation of magnetic domains on FePt thin films. IEEE Transactions on Magnetics, 60(9), pp.1-5.

[65] Smith, D.O., 1956. Magnetization reversal in thin films. Physical Review, 104(5), p.1280.

[66] Yang, F., Feng, Q., Xia, Z., Lu, Q., Song, Y., Huang, S., Zhang, X., Jiang, D., Deng, H., Zeng, Z. and Niu, H., 2021. The existence and origin of field-induced ferrimagnetic order transition of LuFe2O4 single crystal. J. Alloys Compd., 860,

p.158426.

[67] Perzanowski, M., Chojenka, J., Szkudlarek, A. and Krupinski, M., 2024. Magnetization reversal process in flat and patterned exchange-biased CoO/[Co/Pd] thin films. Acta Mater., 276, p.120129.

[68] Hartmann, U., 1999. Magnetic force microscopy. Annu. Rev. Mater. Sci., 29(1), pp.53-87

[69] Fairley, N., Fernandez, V., Richard-Plouet, M., Guillot-Deudon, C., Walton, J., Smith, E., Flahaut, D., Greiner, M., Biesinger, M., Tougaard, S. and Morgan, D., 2021. Systematic and collaborative approach to problem solving using X-ray photoelectron spectroscopy. Appl. Surf. Sci. Adv., 5, p.100112.

[70] Saroj Kumar Mishra, Keerthana P., Yukiko K.Takahashi, J.Mohanty,2026. Growth rate induced modulation of perpendicular magnetic anisotropy and domain dynamics in ferrimagnetic TbFe thin film. Surfaces and Interfaces,88,P.109114

[71] Born, A., Decker, R., Buchner, R., Haverkamp, R., Ruotsalainen, K., Bauer, K., Pietzsch, A. and Fohlisch, A., 2021. Thresholding of the Elliott-Yafet spin-flip scattering in multi-sublattice magnets by the respective exchange energies. Scientific reports, 11(1), p.1883.

[72] Carva, K., Battiato, M., Legut, D. and Oppeneer, P.M., 2013. Ab initio theory of electron-phonon mediated ultrafast spin relaxation of laser-excited hot electrons in transition-metal ferromagnets. Physical Review B—Condensed Matter and Materials Physics, 87(18), p.184425.

[73] Ostler, T.A., Barker, J., Evans, R.F.L., Chantrell, R.W., Atxitia, U., Chubykalo-Fesenko, O., El Moussaoui, S., Le Guyader, L.B.P.J., Mengotti, E., Heyderman, L.J. and Nolting, F., 2012. Ultrafast heating as a sufficient stimulus for magnetization reversal in a ferrimagnet. Nature communications, 3(1), p.666.

[74] Radu, I., Vahaplar, K., Stamm, C., Kachel, T., Pontius, N., Durr, H.A., Ostler, T.A., Barker, J., Evans, R.F.L., Chantrell, R.W. and Tsukamoto, A., 2011. Transient ferromagnetic-like state mediating ultrafast reversal of antiferromagnetically coupled spins. Nature, 472(7342), pp.205-208.

[75] Dusabirane, F., Leckron, K., Rethfeld, B., and Schneider, H.C., 2026. Interplay of electron-magnon scattering and spin-orbit induced electronic spin-flip scattering in a two-band Stoner model. Physical Review B, 113(10), p.104403.